Including debris cover effects in a distributed model of glacier ablation

T. D. Reid,[1] M. Carenzo,[2] F. Pellicciotti,[2] and B. W. Brock[3]

Received 19 March 2012; revised 11 July 2012; accepted 18 July 2012; published 20 September 2012.

[1] Distributed glacier melt models generally assume that the glacier surface consists of bare exposed ice and snow. In reality, many glaciers are wholly or partially covered in layers of debris that tend to suppress ablation rates. In this paper, an existing physically based point model for the ablation of debris-covered ice is incorporated in a distributed melt model and applied to Haut Glacier d'Arolla, Switzerland, which has three large patches of debris cover on its surface. The model is based on a 10 m resolution digital elevation model (DEM) of the area; each glacier pixel in the DEM is defined as either bare or debris-covered ice, and may be covered in snow that must be melted off before ice ablation is assumed to occur. Each debris-covered pixel is assigned a debris thickness value using probability distributions based on over 1000 manual thickness measurements. Locally observed meteorological data are used to run energy balance calculations in every pixel, using an approach suitable for snow, bare ice or debris-covered ice as appropriate. The use of the debris model significantly reduces the total ablation in the debris-covered areas, however the precise reduction is sensitive to the temperature extrapolation used in the model distribution because air near the debris surface tends to be slightly warmer than over bare ice. Overall results suggest that the debris patches, which cover 10% of the glacierized area, reduce total runoff from the glacierized part of the basin by up to 7%.

Citation: Reid, T. D., M. Carenzo, F. Pellicciotti, and B. W. Brock (2012), Including debris cover effects in a distributed model of glacier ablation, *J. Geophys. Res.*, *117*, D18105, doi:10.1029/2012JD017795.

1. Introduction

[2] Mountain glaciers are important in several regions of the world as reservoirs for water supply and hydroelectricity generation, and have obvious aesthetic qualities that benefit tourism. However, the international scientific community has reported widespread glacier retreat in recent decades; indeed the Fourth Assessment Report of the Intergovernmental Panel on Climate Change reported that mountain glaciers and snow cover have declined on average in both hemispheres [*Intergovernmental Panel on Climate Change*, 2007]. As well as maintaining large-scale observation networks and data inventories to monitor global trends in glacier activity [*Braithwaite*, 2002; *Zemp et al.*, 2009], it is useful to develop detailed, physically based models of individual glaciers, to provide predictions for local people and test the validity of assumptions used in larger scale studies. Several authors have used a distributed modeling approach for this, whereby a digital elevation model (DEM) of the glacier and its surrounding terrain are used alongside local meteorological data to calculate the energy balance, and thereby ablation, at every point on the glacier surface defined by a pixel in the DEM [*Arnold et al.*, 1996; *Klok and Oerlemans*, 2002; *Dadic et al.*, 2008; *Arnold et al.*, 2006; *Michlmayr et al.*, 2008; *Anslow et al.*, 2008; *Reijmer and Hock*, 2008; *Rye et al.*, 2010; *B. Andersen et al.*, 2010; *M. L. Anderson et al.*, 2010; *MacDougall and Flowers*, 2011].

[3] However, the glacier surface itself may experience important physical changes. In particular, several authors have reported the expansion of glacial debris covers in recent decades in major mountain ranges including the European Alps [*Kellerer-Pirklbauer*, 2008], the Caucasus [*Popovnin and Rozova*, 2002; *Stokes et al.*, 2007], the Himalaya [*Bolch et al.*, 2008; *Shukla et al.*, 2009], and the Southern Alps of New Zealand [*Kirkbride*, 1993]. Debris-covered glaciers are particularly common in the Hindu Kush-Himalayan chain, where pressures on freshwater supply are particularly intense [*Scherler et al.*, 2011]. Since the work of *Østrem* [1959] it is well-known that such debris cover has significant effects on glacier ablation, and recent work shows that debris cover reduces mass balance sensitivity to climatic change [*Anderson and Mackintosh*, 2012]. Very shallow layers of debris enhance melt rates by lowering the surface albedo, and thicker layers suppress melt rates by reducing the amount of surface heat conducted to the ice. Such effects have never, to our knowledge, been explicitly

[1]School of Geosciences, University of Edinburgh, Edinburgh, UK.
[2]Institute of Environmental Engineering, ETH Zurich, Zurich, Switzerland.
[3]School of the Built and Natural Environment, Northumbria University, Newcastle, UK.

Corresponding author: T. Reid, School of Geosciences, University of Edinburgh, EH9 3JN Edinburgh, UK. (tim.reid@ed.ac.uk)

0148-0227/12/2012JD017795

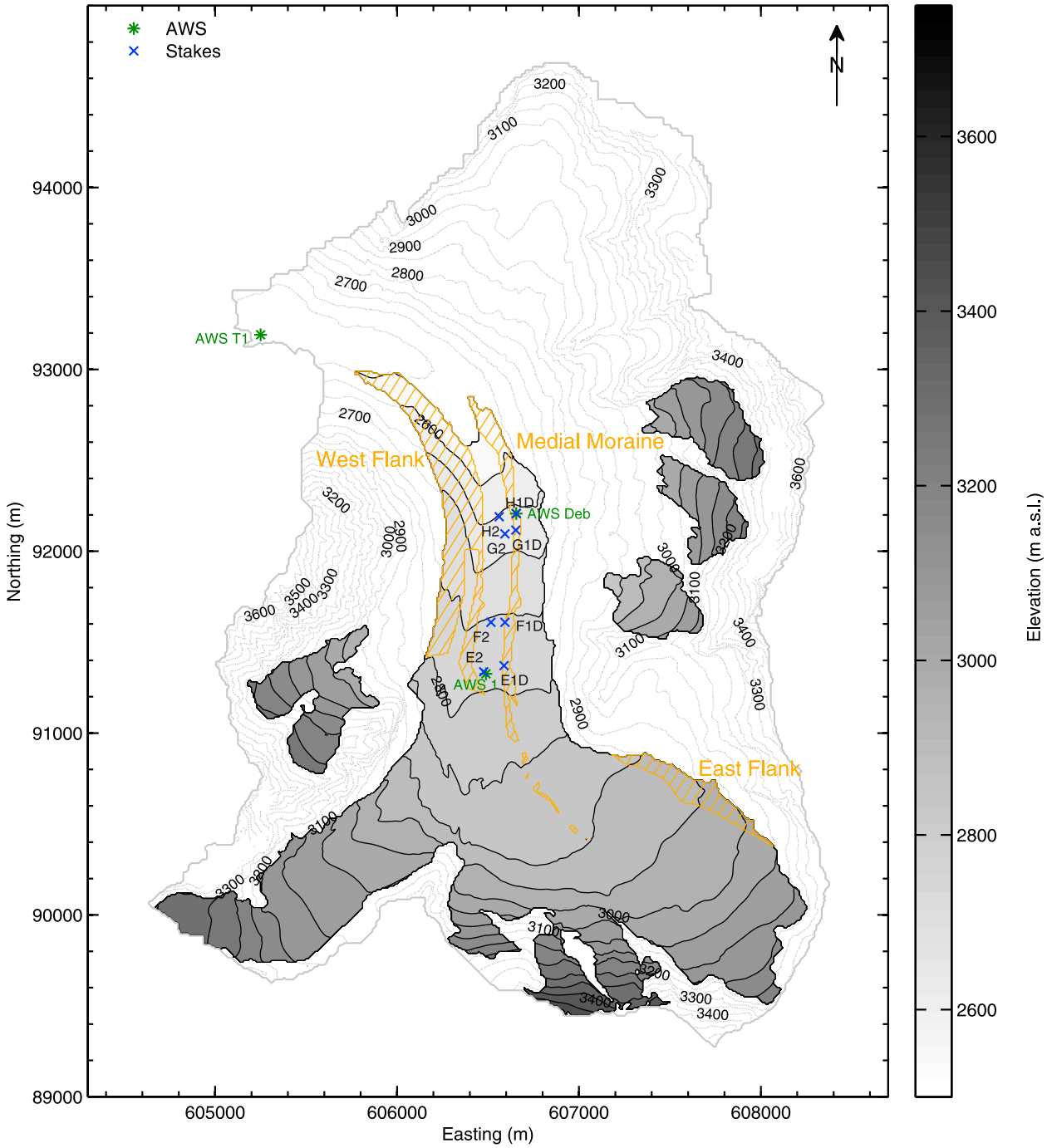

Figure 1. Map of Haut Glacier d'Arolla. Grey areas are glacier and the outer boundary represents the watershed, based on a digital elevation model from a LiDAR flight in October 2010 flown by Helimap System SA. Positions of automatic weather stations (AWS) and ablation stakes are shown. Yellow hatching represents areas of debris covered glacier ice, where debris thickness was comprehensively surveyed at 10 m intervals along east-west transects separated by approximately 30 m northing.

included in a distributed glacier melt model; existing models tend only to apply energy balance equations appropriate for bare ice and snow. Point models exist for debris-covered ice; for example *Reid and Brock* [2010] expanded on the work of *Nakawo and Young* [1981], *Nicholson and Benn* [2006], and *Brock et al.* [2010] to produce a detailed scheme for calculating energy fluxes at the top of a debris layer and heat conduction through the debris layer to the ice below. Such schemes should arguably be used in distributed models for pixels in which debris cover is known to persist.

[4] In this paper, we describe a distributed melt model for Haut Glacier d'Arolla, Switzerland, which has patches of

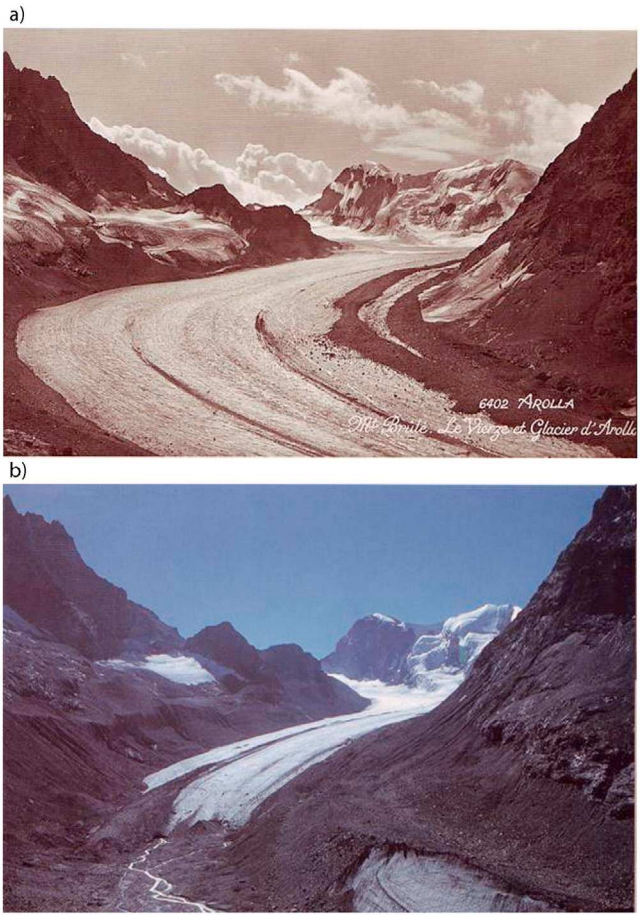

Figure 2. Photographs of Haut Glacier d'Arolla taken from approximately the same site in (top) 1948 (source unknown) and (bottom) 2003 (taken by the authors), showing the glacier retreat and emergence of extensive debris cover on the snout and medial and lateral moraines.

rocky debris covering about 10% of its area. In the model, every pixel of the glacier DEM is defined as either bare ice or debris-covered ice, and debris-covered pixels are prescribed debris thickness values based on a widespread manual survey. A bare ice energy balance model is used for bare ice pixels, while the *Reid and Brock* [2010] model is applied to debris-covered pixels.

2. Study Site and Data

2.1. Haut Glacier d'Arolla

[5] Haut Glacier d'Arolla is a north-facing valley glacier in southwest Switzerland extending from elevations of 2500 to 3600 m. The catchment area of the Arolla basin is approximately 13 km^2, of which about 5.3 km^2 is glacierized [*Dadic et al.*, 2008]. The area has been the subject of several studies which concur that the glacier has exhibited a negative mass balance and extensive retreat over at least the past 50 years [*Oerlemans et al.*, 1998; *Hubbard et al.*, 1998; *Brock et al.*, 2000a]. Furthermore, the glacier has seen the emergence and expansion of three distinct patches of debris in recent decades: a west lateral moraine and medial moraine on the tongue, and an east lateral moraine in the upper basin (Figure 1). The east lateral moraine is a product of rockfall directly onto the glacier surface, the medial moraine is largely derived from melt out of englacially transported material, while the west lateral moraine is thought to contain a mixture of both rockfall and englacial melt-out debris. The three areas now cover about 10% of the total glacierized area. Photographic records indicate that the debris cover near the tongue of the glacier emerged as the glacier retreated over the past 60 years (Figure 2). It is likely that the retreat of Haut Glacier d'Arolla is at least partly the cause of this increase in debris cover, as surface lowering has exposed englacial debris bands and supraglacial transport rates have decreased.

2.2. Data Collection

[6] A series of field campaigns in the summer of 2010 provided the majority of data used for modeling in this paper. Weather stations were deployed from 23 May to 9 September on the ice surface near the center of the glacier (marked as AWS 1 in Figure 1) and on the debris-covered medial moraine near the glacier tongue (AWS Deb). These recorded air temperature, relative humidity, upwelling and downwelling longwave radiation (at AWS Deb only), incoming and outgoing shortwave (SW) radiation, air pressure, wind speed and wind direction with 5 second sampling and 5 minute datalogging; these were averaged to hourly values for modeling. Instrument details are given in Tables 1 and 2. Solid and liquid precipitation is measured at the permanent weather station (AWS T1) situated in the proglacial valley approximately 1 km from the glacier tongue (Figure 1).

[7] During the first field campaign in May there was over 2 meters of snow cover on most of the glacier surface. Four 6-meter ablation stakes - marked E2 (beside AWS 1), F2, G2 and H2 - were inserted along the centreline of the glacier using a Heuke steam drill to get through both snow and ice (further stake transects A, B, C and D were deployed on the upper glacier but are not referred to in this paper). It was not possible to insert ablation stakes on the debris-covered ice at this time because the drill could not get through the debris layer, and digging snow away to clear debris would affect the natural processes occurring. Instead stakes were installed on 28 July at sites on the medial moraine at approximately

Table 1. Technical Characteristics of the Meteorological Sensors Mounted on AWS 1

Variable Measured	Manufacturer	Sensor	Accuracy	Range
Temperature	Rotronic	MP-103A	±0.3°C	−40–60°C
Relative humidity	Rotronic	MP-103A	±1%	0–100%
Shortwave radiation	Kipp and Zonen	CM7B	±5%	305–2800 nm
Net radiation	Kipp and Zonen	NR Lite	±15%	0.2–100 μm
Wind speed	Young	S-WMON	±0.3 m s^{-1}	1–60 m s^{-1}
Wind direction	Young	S-WMON	±3°C	0–360°C

Table 2. Technical Characteristics of the Meteorological Sensors Mounted on AWS Deb

Variable Measured	Manufacturer	Sensor	Accuracy	Range
Temperature	Vaisala	QMH101	±0.3°C	−40–60°C
Relative humidity	Vaisala	QMH101	±1%	0–100%
Shortwave radiation	Kipp and Zonen	CM7B	±5%	305–2800 nm
Wind speed	Vaisala	WMT50	±2.5 m s^{-1}	1–60 m s^{-1}
Wind direction	Vaisala	WMT50	±3°C	0–360°C

the same elevations as the bare ice stakes. The debris stakes were marked E1D, F1D, G1D and H1D (beside AWS Deb) and were installed by carefully clearing a patch of debris cover, drilling the hole in the exposed ice, inserting the ablation stake and rebuilding the debris layer as naturally as possible. Debris thickness was also recorded at each stake.

[8] In 2010, a manual survey of the medial moraine produced 127 measurements of debris thickness on eight equal-elevation transects. These consisted of measurements 2 m apart on eight separate east-west transects of the debris patch; the transects were separated by a north-south distance of 200 m. The later analysis of ablation stake data, which indicated the effects of the debris, prompted a more widespread survey in 2011, taking into account all three debris areas: the medial moraine, the lower west flank and the higher east flank (yellow-hatched areas in Figure 1). Masks of the three main debris areas were created after a comprehensive manual survey using a handheld GPS. Debris thickness, d, was sampled at 10 m intervals along east-west transects separated by approximately 30 m northing. Small holes were created by carefully removing debris to expose the ice, and d was measured as the mean of five ruler depth measurements along the south side of each hole, from lowest observed depth in the ice to the apparent top of the debris.

[9] An airborne LiDAR flight over the Arolla glacier basin in October 2010 by Helimap System SA provided a DEM with a grid resolution of 10 m, which is used as the basis of the models in this paper.

3. Model Development

3.1. Distributed Setup

[10] The distributed model solves energy balance models (EBMs) for snow, bare ice and debris-covered ice, considering every pixel in the Arolla basin DEM. An hourly timestep is used. On each timestep the DEM is used to determine which pixels are shaded by topography and which are not. A model of potential clear-sky radiation [*Pellicciotti et al.*, 2011] is used to calculate the theoretical ratio between diffuse and direct SW radiation for the glacier area. This ratio is used to compute direct and diffuse SW radiation for the AWS 1 site from the station measurements, which are adjusted using the sky view factor for the site and a first estimation of reflected radiation based on the ratio of pixels in and out of topographic shade. These values are then distributed over the catchment according to the topography, sky view factor and surface conditions (mean albedo catchment) of each pixel [*Corripio*, 2002].

[11] The hourly meteorological data from AWS 1 are distributed across the glacier to drive the EBMs. An air temperature lapse rate of 2.5°C km^{-1} was determined using measurements from three AWSs deployed along the centreline of the glacier in 2001 [*Carenzo et al.*, 2011] and used in the model to extrapolate AWS 1 data. These are used in the three EBM routines to compute hourly energy fluxes in W m^{-2}. Relative humidity and wind speed are assumed constant across the glacier surface. Incoming longwave radiation is parameterized using the approach of *Swinbank* [1963] corrected for the cloud type and amount following *Lhomme et al.* [2007]. Outgoing longwave radiation is calculated from the Stefan-Boltzman law, assuming a surface emissivity of 1. Precipitation data from AWS T1 was identified as either rain or snow by assuming a fixed threshold temperature of 1°C; this value was best at reproducing albedo peaks and therefore identifying snowfall events. Uniform deposition maps (no precipitation lapse rate) are assumed.

[12] For every 10 m pixel in the rectangular DEM (475 pixels east by 595 pixels north), a value is assigned according to a glacier mask G_{xy} that classifies each pixel as not glacier ($G_{xy} = 0$), bare glacier ice ($G_{xy} = 1$) or debris-covered glacier ice ($G_{xy} = 2$). A snow depth mask S_{xy} based on start-of-season observations is superimposed, and on each timestep the appropriate EBM is used to calculate ablation for the pixel. For a snow covered pixel, once all the snow is melted the model reverts to using either the bare ice or debris EBM, depending on the pixel classification from the underlying debris mask. Accordingly at any timestep the melt rate for a pixel at position x, y is:

$$M_{xy} = \begin{cases} 0 & \text{if } G_{xy} = 0 \\ M_{xy,s} & \text{if } G_{xy} = 1 \text{ and } S_{xy} > 0 \\ M_{xy,i} & \text{if } G_{xy} = 1 \text{ and } S_{xy} = 0 \\ M_{xy,i} & \text{if } G_{xy} = 2 \text{ and } S_{xy} > 0 \\ M_{xy,d} & \text{if } G_{xy} = 2 \text{ and } S_{xy} = 0 \end{cases} \quad (1)$$

where $M_{xy,s}$, $M_{xy,i}$ and $M_{xy,d}$ are the melt rates for snow, bare ice and debris-covered ice, respectively, described in the next section.

3.2. Surface EBMs

[13] The EBMs for snow and ice are partly based on those described in *Corripio* [2002], *Dadic et al.* [2008] and *Carenzo et al.* [2011]. The energy balance is computed by assuming a one-dimensional system (atmosphere - glacier surface - subsurface snow or icepack) and the heat conduction is simplified by using a two-layer subsurface model [*Pellicciotti et al.*, 2009]. It is assumed that the energy fluxes at the glacier-atmosphere interface are entirely absorbed by the top layer in the case of ice, but in snow 64% of the net SW radiation flux can penetrate the surface and reach the second layer. The snow temperatures are derived by solving the differential equation of heat conduction at each layer, with a bottom boundary condition determined by the weekly

Table 3. Thermal Conductivity of Debris, k_d, in W m^{-1} K^{-1} Calculated for Stake H1D Using Equation (7) for the Two Measured Debris Thickness (d) Values, Over Two Different Periods in 2010, and Considering an Error of ±5 cm in Measured Ablation, M

	Period 28/07 to 29/08			Period 29/08 to 11/09		
d	M − 5 cm	M	M + 5 cm	M − 5 cm	M	M + 5 cm
6 cm	0.95	1.01	1.07	0.99	1.03	1.07
5 cm	0.84	0.89	0.95	0.88	0.92	0.96

running mean of the air temperature (though with a maximum possible value of 0°C) - this accounts for the atmospheric influence on the temperature of the snowpack. For both snow and ice, the energy available for melt, Q_M, is the sum of the energy fluxes at the snow or ice surface (note subscripts xy are not used on the right hand side for neatness):

$$Q_{M,xy,s} = Q_{M,xy,i} = Q_I + L_{net} + Q_H + Q_{LE} + Q_R + Q_C \quad (2)$$

where Q_I is net SW radiation, calculated using an appropriate value of albedo for either ice or snow. L_{net} is net longwave radiation, Q_H and Q_{LE} are sensible and latent heat fluxes, Q_R is heat flux supplied by rain and Q_C is conductive heat flux into the snow or ice. Hourly melt rate (m w.e. h^{-1}) for the pixel is then:

$$M_{xy,s} = M_{xy,i} = \frac{Q_M \Delta t}{\rho_w L_f} \quad (3)$$

where Δt is the model timestep (1 hour), L_f is the latent heat of fusion for water and ρ_w is the density of water. Snow albedo is computed from accumulated daily maximum positive air temperature since the last snowfall, following the model of *Brock et al.* [2000b], and ice albedo is set to a constant value of 0.2, which is the mean value from measurements [*Pellicciotti et al.*, 2005; *Strasser et al.*, 2004].

[14] The debris energy balance is calculated according to the model of *Reid and Brock* [2010] - for a detailed description please see that paper. The sum of energy fluxes at the surface is essentially the same as equation (2), but because debris does not melt the debris surface temperature T_s is assumed to change such that these fluxes sum to zero:

$$Q_I + L_{net}(T_s) + Q_H(T_s) + Q_{LE}(T_s) + Q_R(T_s) + Q_C(T_s) = 0 \quad (4)$$

[15] Equation (4) is solved for T_s using a numerical Newton-Raphson method. Conduction through the debris is then calculated using a Crank-Nicholson scheme with intermediate temperature layers each 1 cm thick, and boundary conditions determined by the newly calculated T_s and the temperature of the debris-ice interface, which is assumed to stay at 0°C. The ablation rate is determined from the conductive heat flux to the ice $Q_{C,base}$, found using the temperature gradient between the lowest of the 1 cm debris layers and the ice:

$$M_{xy,d} = \frac{Q_{C,base} \Delta t}{\rho_w L_f} \quad (5)$$

where:

$$Q_{C,base} = -k_d \left(\frac{dT_d}{dz} \right)_{base} \quad (6)$$

[16] T_d is debris temperature, z is depth below the surface and k_d is debris thermal conductivity. It should be noted that caveats are imposed on equations (3) and (5) such that there can of course never be negative melt rates; if the equation produces a negative number then the melt rate is set to zero. Debris albedo is set to a constant value of 0.13 [*Reid and Brock*, 2010].

3.3. Debris Thermal Conductivity

[17] As explained in *Brock et al.* [2010] estimates of k_d (W m^{-1} K^{-1}) can be obtained from field data by solving the Fourier heat conduction equation and assuming all heat conducted to the base of the debris is consumed in melting ice. This requires measured ablation under debris M_d (m) and the debris temperature profile $\frac{dT_d}{dz}$ (K m^{-1}) in order to estimate k_d for individual sites using:

$$M_d \approx -\frac{k_d \Delta t}{\rho_w L_f} \frac{dT_d}{dz} \approx -\frac{k_d \Delta t}{\rho_w L_f} \frac{T_f - T_s}{d} \quad (7)$$

where Δt (s) is the elapsed time, T_f (K) is the temperature at the debris-ice interface, T_s (K) is the debris upper surface temperature and d (m) is the debris layer thickness. This approximation requires a linear profile of temperature with depth in the debris layer, which is a justifiable assumption on long timescales [*Nicholson and Benn*, 2006; *Brock et al.*, 2010; *Reid and Brock*, 2010].

[18] To estimate k_d for Arolla two Tinytag temperature loggers (0.2 K precision), with two sensors on each logger, were installed in close proximity to ablation stake H1D, where the debris thickness was measured as 6 cm. The temperature sensors were attached to the tops and bottoms of two selected stones of thickness (d) equal to 5 and 6 cm. It is difficult to measure T_s accurately [*Brock et al.*, 2010], but for this study sensors were attached to the flat tops of the two clasts using reflective tape so that they were as near as possible to the surface, while also mostly shaded from heating by direct solar radiation. The other two sensors were placed on the ice and the clasts placed on top in order to measure T_f. The sensors measured temperature at 15 minute intervals, which were averaged into hourly values.

[19] Table 3 shows twelve calculated values of k_d for the site, using ablation derived from stake readings (considering an uncertainty of ±5 cm in the reading), the two different measured values of d, and averaged $T_s - T_f$. Temperature inversions with $T_s < T_f$ were observed on just under 20% of datapoints, however these inversions had a median value of just 0.5 K, and given that they don't contribute to ablation those points were discarded from the analysis. The calculation was performed for two periods in 2010, namely 28/07 to 29/08 and 29/08 to 11/09. The mean using this approach is $k_d = 0.96$ W m^{-1} K^{-1}, close to the value of 0.94 W m^{-1} K^{-1} determined for Miage glacier, Italy, by *Brock et al.* [2010]. Those authors calculated their value of k_d based on measurements at many more sites with a variety of debris-layer structures, so their value is arguably more suitable for glacier-wide

Table 4. Number of Measurements (N), Mean (μ) and Standard Deviation (σ) of Debris Thickness on the Three Main Debris Patches (Medial Moraine (MM), West Flank (W) and East Flank (E)) and Over All Three Patches

Area	MM	W	E	All
N	686	239	133	1058
μ (cm)	5.00	3.41	14.48	5.83
σ (cm)	9.66	8.04	20.96	11.88

application; moreover they adjusted surface thermistor values - which may be affected by solar heating - using radiative temperature measurements. The Arolla and Miage glaciers are only about 50 km apart in the Alps, and have debris covers made from similar rock types. For these reasons, it was deemed appropriate to apply k_d = 0.94 W m^{-1} K^{-1} for all calculations in this paper. This value makes intuitive sense for clasts with air pockets, lying between thermal conductivities for granite (1.7 to 4.0 W m^{-1} K^{-1}) and air (0.024 W m^{-1} K^{-1}).

[20] The *Reid and Brock* [2010] model requires values for other characteristics of the debris layer including density, specific heat capacity, emissivity, albedo and aerodynamic roughness length. In the absence of other information, this paper adopts the same values that *Reid and Brock* [2010] applied to the Miage glacier, which again seems justifiable given the relatively close proximity of the two glaciers and similar surrounding lithology. *Reid and Brock* [2010] showed via a sensitivity analysis that varying the thermal conductivity had more significant effects on the model results than any of the other parameters; this was confirmed through sensitivity runs on the distributed model described in this paper (results not shown).

[21] It could be argued that the spatial parameterization of aerodynamic roughness length should become more complex over a patchy, discontinuous debris cover such as Arolla, especially at the transition zones between bare and debris-covered ice. The surface roughness is likely affected by the size, shape and distribution of clasts in the debris layer, and the complex topography created by raised areas where debris has suppressed ablation. Further investigations could examine these issues but would require detailed micrometeorological information which is beyond the scope of this current study, so we retain a constant value for the purposes of modeling.

3.4. Debris Thickness Distribution

[22] To provide a debris thickness dataset, the medial moraine measurements from 2010 were combined with those of 2011, and the east and west flank data for 2011 were applied to the 2010 models. It is therefore assumed that the debris cover distribution does not change dramatically over the course of a year. All debris thickness values (each resulting from 5 measurements around the edge of a hole dug down to the ice) were rounded to the nearest 1 cm, with 0 cm classified as bare ice. It could be argued that patches of bare ice in an otherwise debris-covered area should be modeled in a different way from bare ice elsewhere, because they might have a lower albedo due to fine-grained particles, or be affected by longwave radiation emitted by surrounding debris-covered topography. However, the number of such pixels was small, and for the purposes of this paper they were modeled in the same way as all the other bare-ice pixels.

[23] A small number of measured values of debris thickness greater than 50 cm were discarded from the dataset for analysis. As shown in Figure 6 and stated by *Brock et al.* [2010], ablation tends to plateau at a low rate under any debris layer thicker than about 20 cm. Also, these high values were generally recorded at boulders on the glacier surface, which were relatively few in number and are not

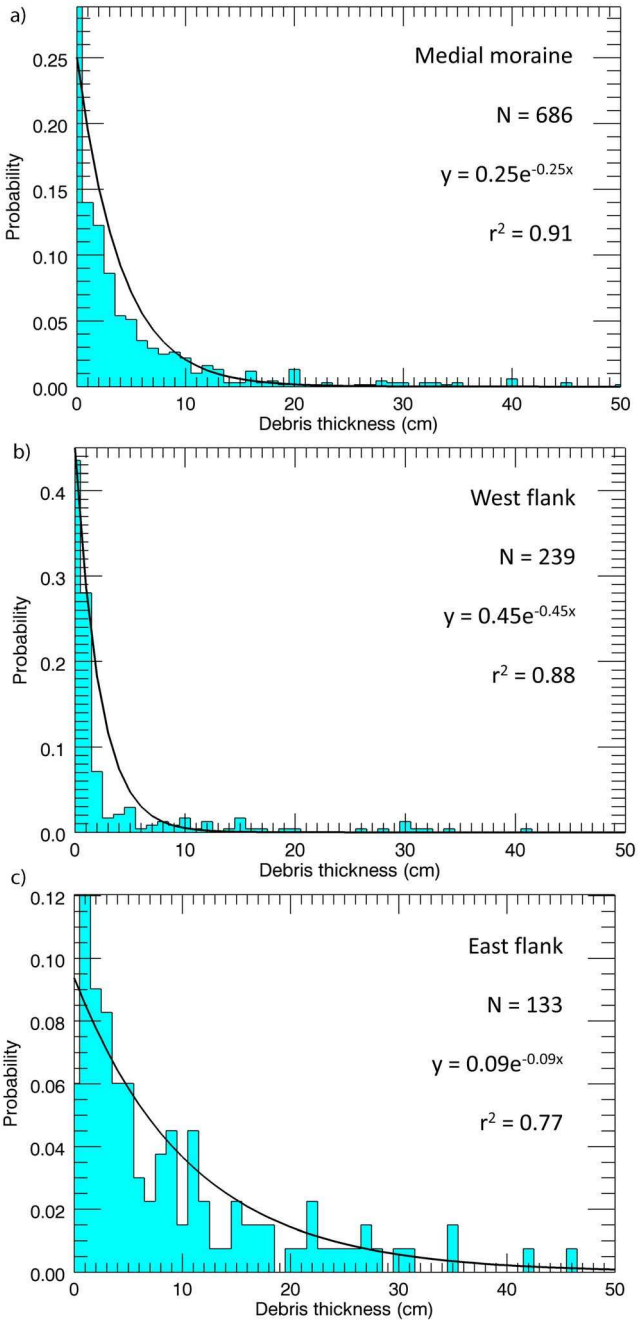

Figure 3. Probability density functions of debris thickness (lines) fitted to data from manual surveys (bars) for the three main debris-covered areas. Included in each is the total number of measurements (N), the equation of the fitted PDF and the r^2 goodness of fit to the measurements.

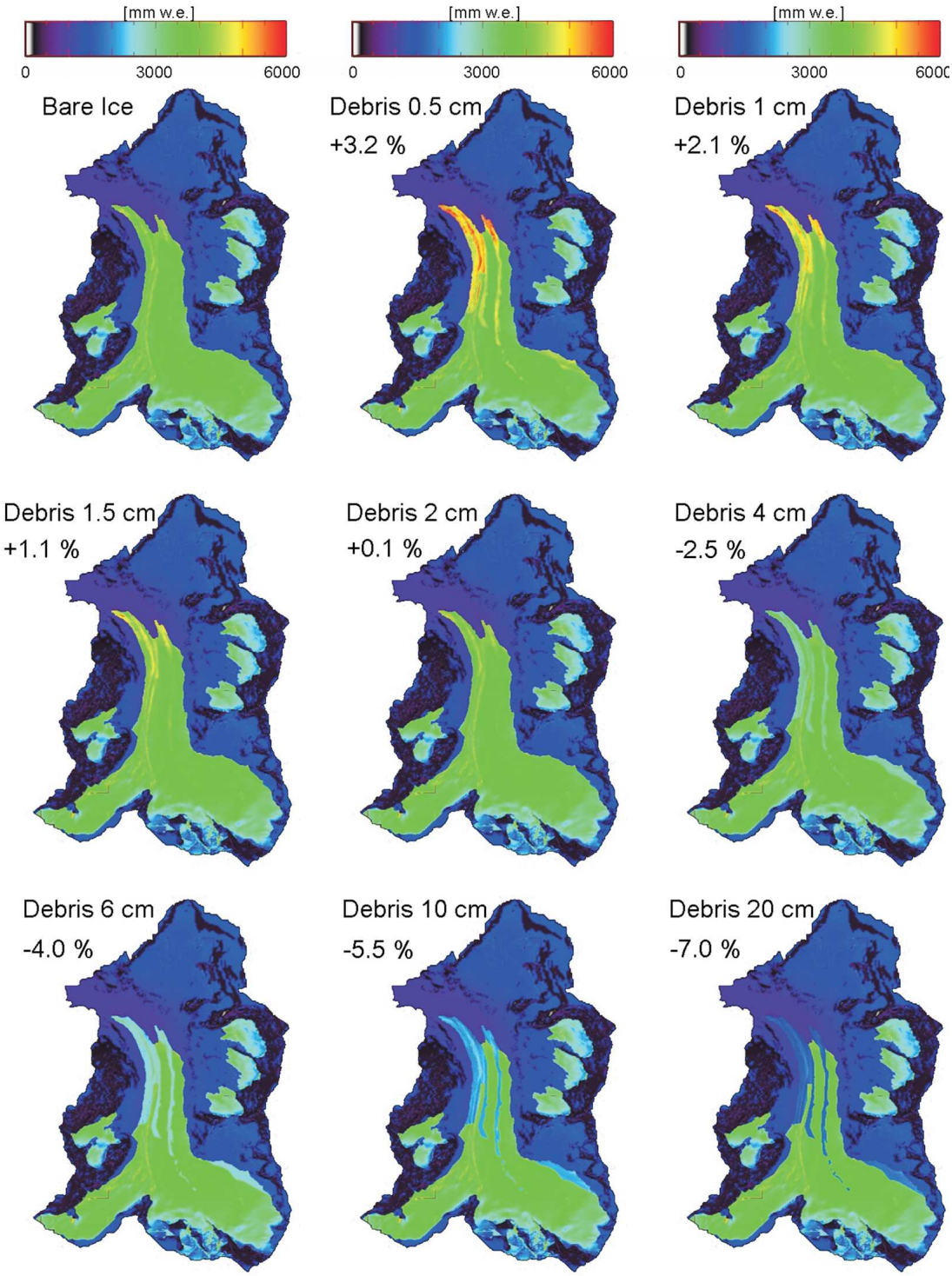

Figure 4. Seasonal ablation across Haut Glacier d'Arolla from 23 May to 9 September 2010 predicted by models assuming bare ice everywhere (top left), then imposing debris layers of increasing thickness in the defined debris areas (see Figure 1). The total calculated melt over the glacierized area assuming bare ice everywhere was 17356600 m^3 w.e.; percentages show the effects on this figure of imposing debris layers.

explicitly accounted for in the model. Such effects are complex, because a boulder very thoroughly shades and preserves a small area of ice, which sometimes evolves into a column with the boulder balanced on top forming a mushroom-like pedestal. However, once the boulder finally slides off it is likely that the bare column of ice would melt away quite rapidly, perhaps compensating for the earlier shading effects.

[24] Table 4 outlines the main statistics for each area. The east flank had by far the thickest average debris cover and

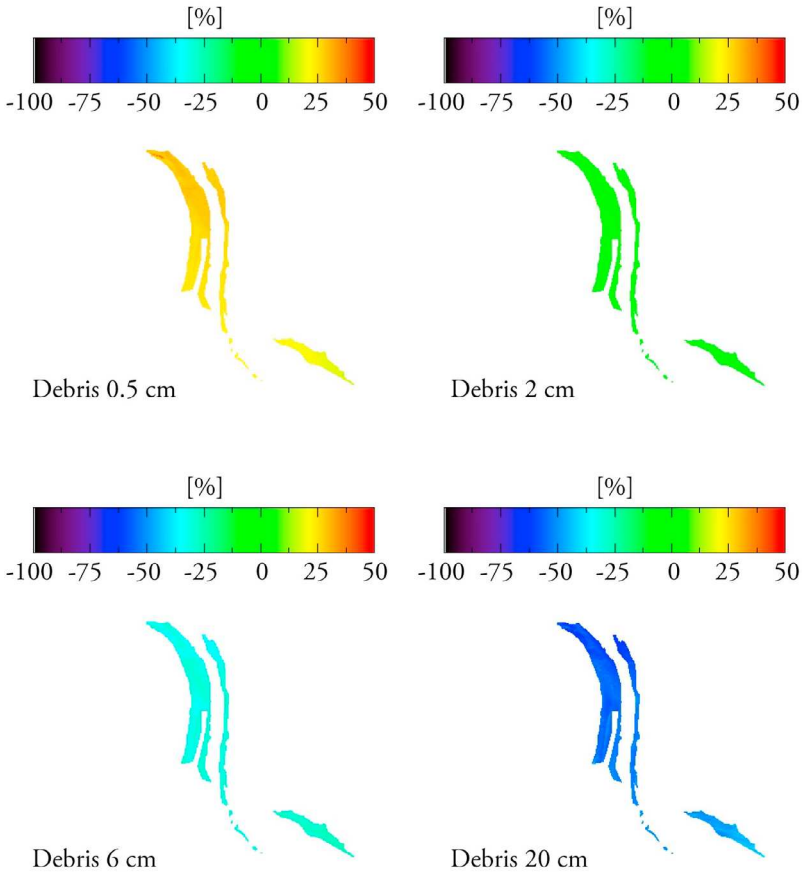

Figure 5. Percentage difference between modeled ablation assuming bare ice everywhere, and imposing debris layers of thickness 0.5, 2, 6 or 20 cm (see Figure 4).

the west flank had the thinnest, while the medial moraine had 5 cm on average.

[25] No significant correlations between elevation and debris thickness were observed. Therefore, given that the down-glacier length of each patch is much longer than the cross-glacier width, and that meteorological variables do not change significantly across the narrow width of each debris patch, we can rule out significant impacts of any spatial autocorrelation in the debris thickness. For these reasons, instead of spatially interpolating the data over a grid, the probabilistic nature of the debris cover was exploited. It was noticed that histograms of the debris thickness data (Figure 3) closely resembled exponential probability distributions (PDF), so these were fitted to the data. The non-parametric Mann-Whitney U test was used to show that the datasets for the three different areas were all statistically significantly different from one another, so for the final model runs the three areas were treated separately. The east flank in particular shows a much wider range of debris thicknesses; this might be generated by rockfalls from the Bouquetins ridge above, whereas the medial moraine and the west flank likely hold debris generated from englacial sources.

[26] Interestingly, the exponential PDF is a special case of the Weibull PDF, which has been used to describe the size distribution of particles generated by fragmentation processes such as grinding, milling and crushing [*Tenchov and Yanev*, 1986]. These seem analogous to the processes that might produce debris on a glacier surface, and one can speculate that the same principles could be applied to the thickness of a debris layer. It seems reasonable to propose that when the debris cover is thin and sparse, as at Arolla, the lateral redistribution of debris by the differential ablation process described earlier would produce gradual settling of debris into wide mounds, with large areas of thin debris and smaller areas of thick debris - hence an exponential PDF. However, when a debris layer becomes continuous, such as at Miage glacier, Italy [*Brock et al.*, 2010], the peak of the curve will not be at low values but rather at the average debris thickness of the glacier, potentially following a bell-shaped Weibull distribution.

4. Results and Discussion

4.1. Using Constant Debris Thickness

[27] For the first model runs, a constant value of debris thickness was applied to all the debris-covered glacier pixels. Based on the manual survey, the mean thickness of debris cover on Haut Glacier d'Arolla was approximately 6 cm, but for purposes of theoretical insight the model was run under conditions assuming a range of values from $d = 0$ (i.e. bare ice everywhere) to 20 cm on the debris mask area defined in Figure 1. Figure 4 shows the distribution of cumulative ablation for summer 2010 over the glacier for this range. Under the bare-ice assumption, the ablation is

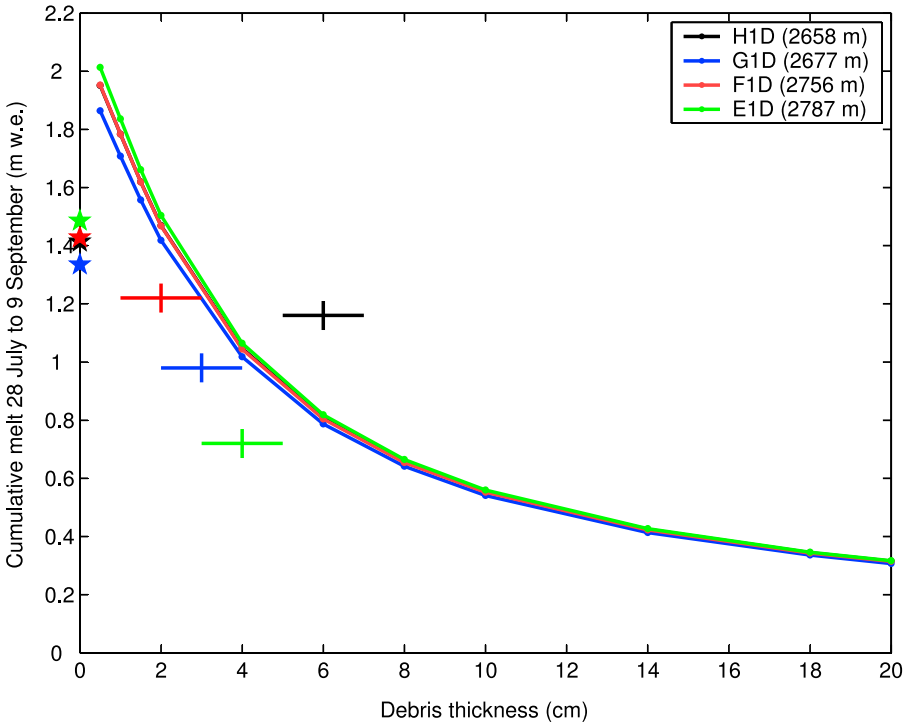

Figure 6. Cumulative ablation from 28 July to 9 September 2010 predicted for the four ablation stake sites on the medial moraine, assuming bare ice everywhere (stars on the vertical axis) and imposing debris layers of increasing thickness (lines). Crosses indicate the actual stake measurements, with the lengths of arms covering the estimated errors of 1 cm in debris thickness measurement and 5 cm in ablation measurement.

fairly uniform over the glacier area, though with some differential melt on the lateral moraine and a slight tendency for increased ablation toward the lower elevations at the glacier tongue, as might be expected. Figure 5 shows the enhancement or reduction of melt for three selected debris thickness values. On adding a thin layer of debris at $d = 0.5$ cm - an unrealistic but useful thought experiment - there is clear enhancement of melt in the debris-covered areas, which is most intense in the lower glacier. At $d = 2$ cm the ablation is very similar to that predicted for bare ice, and on further increasing d the ablation is increasingly suppressed in all the debris-covered areas, by up to 2500 mm water equivalent for $d = 20$ cm. The value at which debris-covered ablation equals bare ice ablation is the so-called critical thickness, and 2 cm is close to values observed on Miage glacier [*Brock et al.*, 2010; *Reid and Brock*, 2010] as well as glaciers in the Himalaya, Canada and Sweden [*Nicholson and Benn*, 2006].

[28] These effects are perhaps more clearly illustrated in Figure 6, which shows the modeled cumulative melt rate for the four debris pixels on the medial moraine in which ablation stakes were deployed, as a function of the imposed debris thickness. The close proximity of the four lines indicates that the model is much more sensitive to debris thickness than the elevational differences in meteorological variables for these four sites. The curves resemble the well-known Østrem curve [*Østrem*, 1959], with thin debris enhancing ablation and thicker debris suppressing it. However, as argued above the very low values of d that dramatically enhance melt are very unlikely to be found over large areas - in reality, thin debris cover tends to be very patchy, with exposed areas of bare ice that reduce the overall effective ablation of the area such that the curve would really be closer to the bare ice melt rate, producing the famous hump of the Østrem curve [*Reid and Brock*, 2010].

[29] Also superimposed on Figure 6 are the real ablation measurements for the stake sites, with estimated errors. The model results pass through the range of measured values. It should be noted that point ablation measurements are being compared to model estimates for 10 by 10 m pixels, within which there may be large variations in debris thickness. The different melt rates associated with these spatial variations could quickly generate local topographical variations, and gravity then redistributes material from relatively high (thicker debris) to low (thinner debris) places. This process of gravity-driven lateral redistribution of debris is likely to operate continuously over shallow debris patches during the melt season.

[30] Figure 7 shows the modeled cumulative ablation for the entire summer season at the bare ice stake sites, with ablation measured on a total of five visits to the glacier. Figure 8 shows the same for the debris stakes, which were deployed from 28 July, for roughly the second half of the period shown in Figure 7. This essentially shows the same results as Figure 6, but highlights how a 1 cm error in debris thickness affects the model predictions.

4.2. Input Data Limitations

[31] The presence of debris cover can be expected to affect local meteorology, mainly by raising the near-surface air

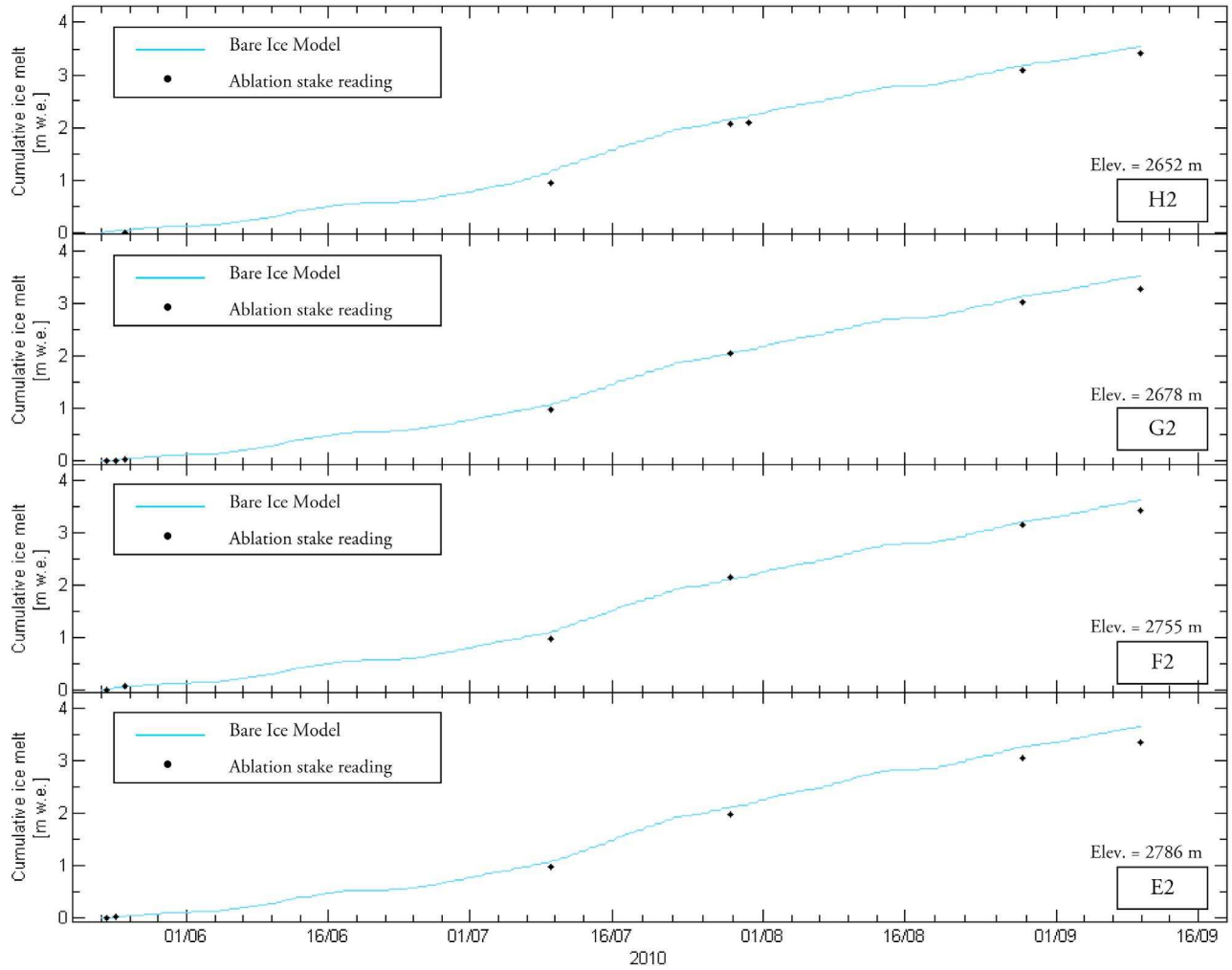

Figure 7. Modeled and measured cumulative ablation from 23 May to 9 September at the four bare-ice ablation stakes close to the medial moraine (see Figure 1).

temperature relative to that above bare ice surfaces during and after sunshine hours. The data from AWS Deb, situated on the medial moraine, provided an opportunity to investigate this. Table 5 shows the results of driving the model with AWS Deb data (instead of using the 2001 lapse rates and AWS 1 data), for the H1D stake site which was right beside AWS Deb. The differences in relative humidity, wind speed, SW and longwave radiation through the two approaches were small, and have very little effect on ablation. However, the temperature recorded at AWS Deb was substantially warmer than predicted by the lapse rate, and using this data as input increases the modeled total seasonal ablation by 18.8% relative to the value using the lapse rate, moving the model prediction closer to the ablation stake data.

[32] Figure 9 shows the daily mean air temperature for the H1D site, as measured at AWS Deb and as modeled using the AWS 1 data with the 2001 clean ice lapse rate. The two temperatures are very close for the first part of the season during which the entire glacier is snow covered. However, as snow melts toward the end of June it is clear that the exposed debris cover is having the effect of raising the AWS Deb air temperature above what one might expect over clean ice. This warming is more pronounced when temperatures are higher, and is likely related to direct solar heating of the debris, which then releases energy to the air as sensible heat or longwave radiation.

[33] Through these methods, on still, sunny days the warm debris surface is creating a near-surface layer of warm air. Alternatively it could be argued that the lapse rate on the glacier is not linear, or varies on a diurnal basis [*Petersen and Pellicciotti*, 2011; *Shea and Moore*, 2010]. Some of the data used to determine the lapse rates in 2001 were collected from much further up the glacier (at 3000 m) than any in this study, so the lapse rate may lose accuracy relative to what exists on the lower parts of the glacier. When a relatively smooth surface such as glacier ice is interrupted by a rougher debris-covered surface, the distance of upwind fetch required for a boundary layer to develop could be considerably smaller than the size of debris patches, leading to a debris-adjusted boundary layer in some areas. Indeed, as air moves from ice across a debris patch an internal boundary layer of greater than 2 m thickness will develop in just a few tens of meters from the debris edge (or even just a few meters under unstable conditions) [*Granger et al.*, 2002]. These complications imply that the variability of meteorological variables across a heterogeneous glacier surface are

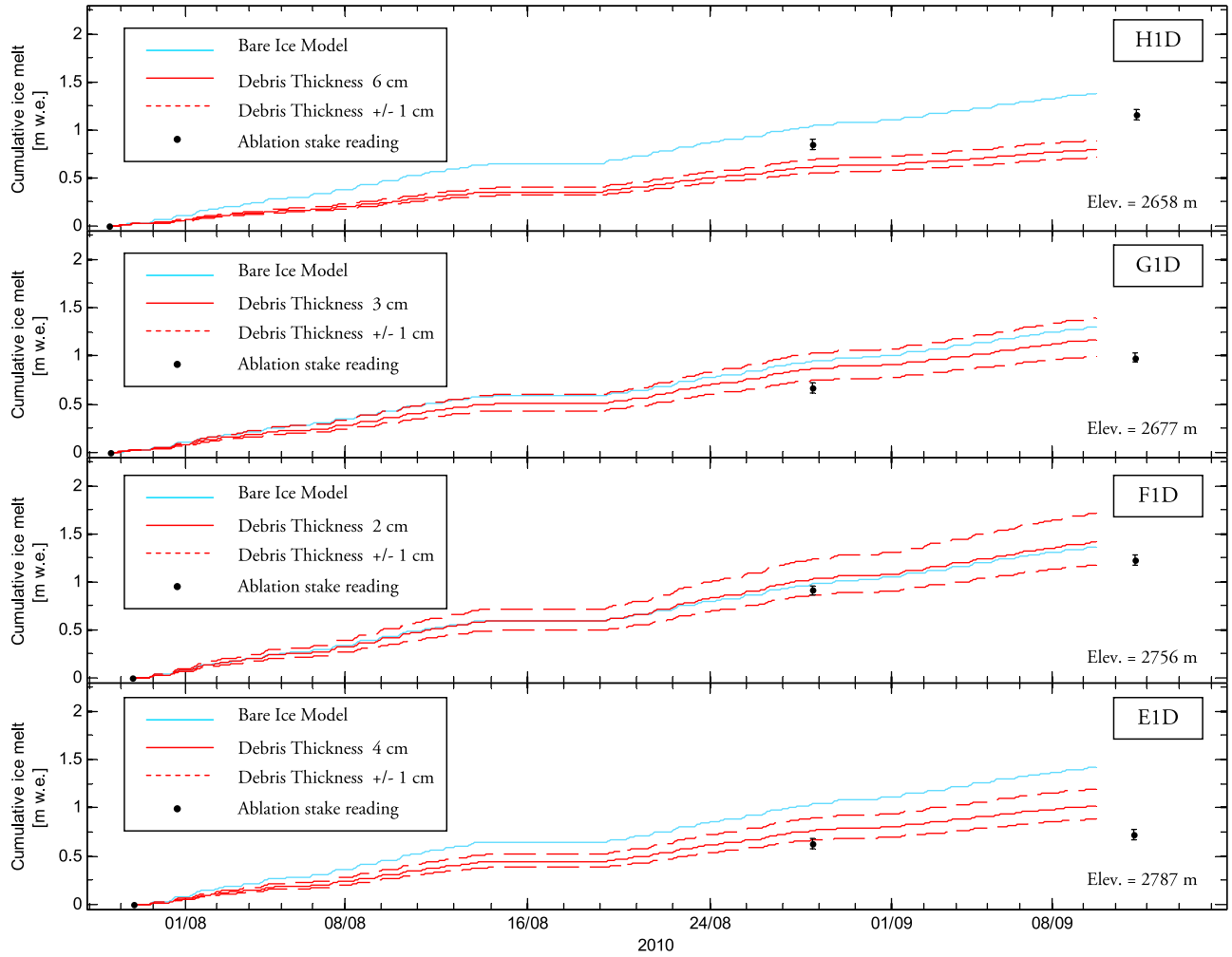

Figure 8. Modeled and measured cumulative ablation from 28 July to 9 September at the four debris-covered-ice ablation stakes on the medial moraine (see Figure 1). Blue line shows the result assuming bare ice, while solid (dashed) red lines show model results with debris thickness equal to the value measured on 28 July (±1 cm). Note that simulations could only be run up to 9 September 2010 because of gaps in the input meteorological data, but the last ablation stake readings were made on 11 September.

an important area for future work. However, such efforts would require much denser networks of meteorological sensors to verify the trends that are occurring. For the remaining distributed modeling results shown in this paper we maintain the use of data solely from AWS 1, with the same lapse rates applied.

4.3. Effects on Heat Fluxes

[34] Figure 10 effectively illustrates why the debris cover has such an impact on ablation, by examining the calculated mean daily cycle of surface temperature for a range of debris thickness from 0 to 20 cm. While a bare ice surface remains at 0°C or close to it during the day, a debris layer is very quickly warmed by solar radiation before cooling back close to zero in the evening. This has significant effects on the upwelling longwave radiation and the sensible heat flux; both become negative during the day, although they are slightly higher than the bare ice at night due to the lower emissivity and higher surface roughness of the debris. For debris layers thicker than about 2 cm, these fluxes cancel out the net SW radiation (not shown) which is enhanced due to the lower albedo of debris, so that the total energy balance is less positive toward the ice and ablation is suppressed.

[35] The outgoing sensible heat flux shown in Figure 10 is high compared to some other studies in alpine/morainal

Table 5. Modeled Cumulative Ablation in Meters on 9 September 2010 at Stake H1D for the Period Shown in Figure 8, With Variables Adjusted From the Baseline Model (Cumulative Ablation Equal to 0.790 m w.e.), Which Uses Data From AWS 1 After Applying the Clean-Ice Lapse Rate Measured in 2001, to Use Data From AWS Deb Instead[a]

Variable	Cum. Ablation (m w.e.)	Difference (%)
Air temperature	0.939	+18.8
Relative humidity	0.788	−0.2
Wind speed	0.787	−0.2
Incoming SW	0.817	+3.4
Downwelling LW	0.774	−2.1

[a]Difference (%) is relative to the baseline model. The stake reading carried out on 11 September was 1.161 ± 0.050 m w.e.

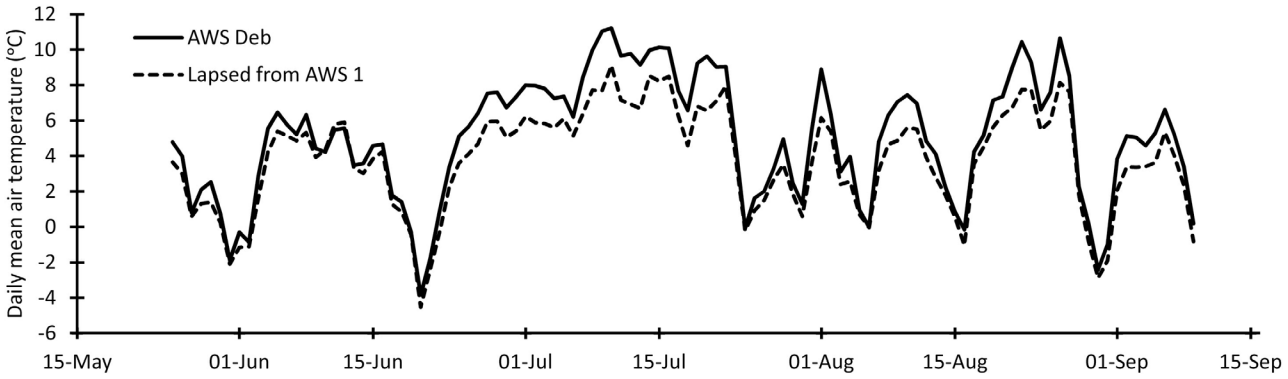

Figure 9. Daily mean air temperature at stake H1D over the 2010 ablation season, as measured at AWS Deb, and as modeled using the 2001 bare-ice lapse from AWS 1 data.

settings [*Kossmann et al.*, 2002; *Turnipseed et al.*, 2002]. However, *Brock et al.* [2010] calculated mean midday sensible heat fluxes in the range 350–400 W m^{-2} over three ablation seasons for a 20 cm debris layer at Miage glacier. Direct comparisons with other studies are difficult because the flux depends on so many factors: temperatures, wind speed, solar radiation, aspect, and the (in)stability correction applied.

4.4. Modeling With Variable Debris Maps

[36] To estimate the present-day overall effects of debris on ablation of the Arolla glacier, a realistic debris cover map was required in the model. To create this, a random debris thickness value was assigned to each pixel that lay in any of the three main debris areas, by randomly sampling from the appropriate fitted PDF in Figure 3. This was repeated 100 times to generate 100 random distributions of debris thickness for the glacier. Because of the large number of pixels involved, this random sampling led to distributions that were quite close to one another. Figure 11 shows the mean predicted cumulative melt over the 100 simulations for the entire glacierized part of the Arolla basin, before and after including the debris cover effects. The runoff reduction caused by the debris layers over the 100 model runs ranged from 6 to 7% for the glacierized area.

5. Concluding Remarks

[37] The effects of debris cover on glacier ablation have been the subject of many studies in recent years, but as far as we are aware this is the first time that a detailed physical model has assigned a specific number for the effects of debris cover on runoff from an entire glacier. It is pertinent to realize that a layer of debris of just 6 cm thickness on average, covering just 10% of the glacierized area could reduce surface runoff by up to 7%. This is largely due to the position of the debris on the glacier tongue, where temperatures are warmest and a bare ice assumption would lead to large amounts of ablation. This highlights the importance of spatially distributing calculations as accurately as possible. For example, a simple temperature index model, adjusted slightly to account for debris and using temperatures measured off-glacier, might overestimate ablation by failing to consider where exactly the debris is having its effect. New physically based techniques for mapping the distribution of supraglacial debris thickness using thermal band satellite imagery [*Foster et al.*, 2012; *Mihalcea et al.*, 2008] are clearly important for the application of our approach to other sites, given the difficulty of measuring debris thickness in the field.

[38] The meteorological lapse rates applied over the glacier surface, which were informed by data from bare ice AWSs, may not be accurate when dealing with areas of debris cover. In reality the debris might affect the near-surface atmosphere to create a very different boundary layer. The spatial distribution of near-glacier air temperature over debris needs to be investigated in a much more detailed and systematic way as an important future priority for distributed modeling.

[39] Another important issue to consider is the impact of thin, sparse debris cover. To what extent do scattered rocks or pebbles affect surface ablation? Anyone who has been on a glacier will have noticed potholes caused by rocks that are too small to shade a large area and so do not create a mushroom pedestal like larger boulders can. The smaller rocks are intensely heated by SW radiation and melt into the ice in a manner similar to cryoconite holes, which are caused by trapped sediment or soot and have been estimated to contribute at least 13% of observed runoff by creating a near-surface hydrological system on one Antarctic glacier [*Fountain et al.*, 2004]. Future work should determine how these effects, and general surface darkening by fine debris, contribute to the heterogeneous debris/ice surface. It is also important to assess how such effects should be scaled up to the size of a 10 by 10 m DEM pixel or even bigger. For example, photographic or remote sensing methods could provide information on patchiness that might inform adjustment of the Østrem curve (Figure 6) for a particular area, through a method similar to that described in *Reid and Brock* [2010].

[40] The data available to validate the model at present is very limited; the model does well at predicting melt rates for four ablation stakes on bare ice and four in the debris-covered area, but these represent only eight individual pixels out of thousands. It would be useful to deploy a wider stake network, and perhaps use airborne LiDAR or stereophotography to acquire detailed DEMs at the beginning and end of

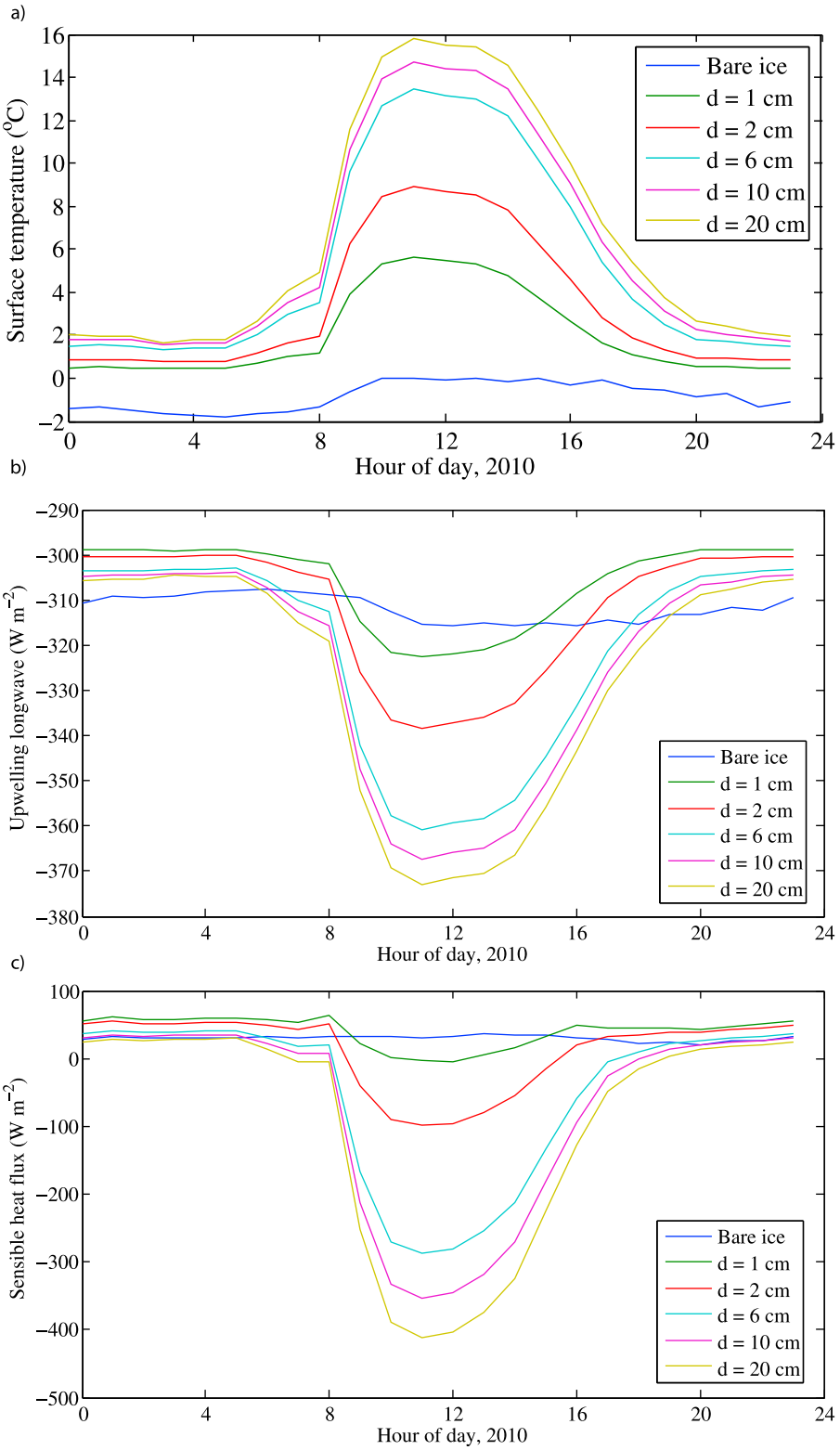

Figure 10. Mean daily cycle of (a) surface temperature, (b) upwelling longwave radiation and (c) sensible heat flux calculated for site H1D assuming bare ice and a range of values for debris thickness. Note a positive flux means toward the ice.

an ablation season, to quantify any widespread differences in surface lowering between bare ice and debris-covered areas.

[41] Despite the limitations described here, the predicted ablation patterns are all qualitatively convincing, and the equations in the model are all based on sound physical and meteorological concepts. We hope that the same framework could be used to predict the effects of debris cover on other glaciers, especially those where there is evidence that the

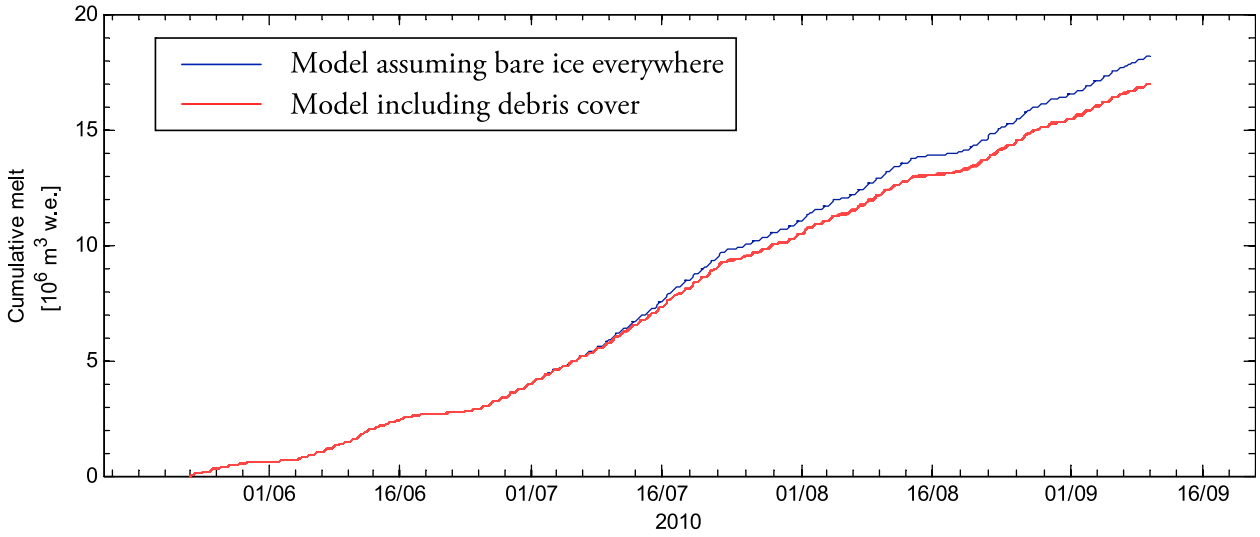

Figure 11. Cumulative melt from 23 May to 9 September 2010 for the entire Arolla glacierized area. Blue line shows results for a model assuming bare ice everywhere, and there are 100 superimposed red lines resulting from superimposing 100 debris maps randomly sampled from Figure 3.

debris-covered area is increasing. Such predictions should prove useful to both local hydrologists and climate scientists.

[42] **Acknowledgments.** M. Carenzo and T. Reid contributed equally to this paper. This work was funded under the EU/FP7 ACQWA (Assessing Climate impacts on the Quantity and quality of WAter) project. The authors would like to thank Lea Müller for her data analysis work and for the plotting routines for some of the figures, as well as Jacopo Sanfilippo, Mauro Bruno, Jakob Helbing, Luca Salvatore, Markus Konz, Inge Juszak, Lena Petersen, Lea Müller, Luzia Sturzenegger, Martin Heynen, Roger Bordoy, Maurizio Savina, Silvan Ragletti, Ilaria Clemenzi, Georgie Bennet and Simone Schauwecker for assistance with fieldwork. Umberto Morra di Cella and Edoardo Cremonese from the Val d'Aosta Environmental Protection Agency kindly provided one AWS for this work. The authors are grateful to Paolo Burlando for supporting the trip to Arolla. The authors also acknowledge Andreas Bauder for providing the 2005 glacier mask. Finally we thank Richard Essery for allowing Tim Reid to spend some of his working hours on this paper, and three anonymous reviewers for very useful comments that greatly improved the manuscript.

References

Anderson, B., and A. Mackintosh (2012), Controls on mass balance sensitivity of maritime glaciers in the Southern Alps, New Zealand: The role of debris cover, *J. Geophys. Res.*, *117*, F01003, doi:10.1029/2011JF002064.

Anderson, B., A. MacKintosh, D. Stumm, L. George, T. Kerr, A. Winter-Billington, and S. Fitzsimons (2010), Climate sensitivity of a high-precipitation glacier in New Zealand, *J. Glaciol.*, *56*(195), 114–128.

Andersen, M. L., et al. (2010), Spatial and temporal melt variability at Helheim Glacier, East Greenland, and its effect on ice dynamics, *J. Geophys. Res.*, *115*, F04041, doi:10.1029/2010JF001760.

Anslow, F. S., S. Hostetler, W. R. Bidlake, and P. U. Clark (2008), Distributed energy balance modeling of South Cascade Glacier, Washington and assessment of model uncertainty, *J. Geophys. Res.*, *113*, F02019, doi:10.1029/2007JF000850.

Arnold, N. S., I. C. Willis, M. J. Sharp, K. S. Richards, and W. J. Lawson (1996), A distributed surface energy-balance model for a small valley glacier. I. Development and testing for Haut Glacier d'Arolla, Valais, Switzerland, *J. Glaciol.*, *42*(140), 77–89.

Arnold, N. S., W. G. Rees, A. J. Hodson, and J. Kohler (2006), Topographic controls on the surface energy balance of a high Arctic valley glacier, *J. Geophys. Res.*, *111*, F02011, doi:10.1029/2005JF000426.

Bolch, T., M. Buchroithner, T. Pieczonka, and A. Kunert (2008), Planimetric and volumetric glacier changes in the Khumbu Himal, Nepal, since 1962 using Corona, Landsat TM and ASTER data, *J. Glaciol.*, *54*(187), 592–600.

Braithwaite, R. J. (2002), Glacier mass balance: The first 50 years of international monitoring, *Prog. Phys. Geogr.*, *26*(1), 76–95.

Brock, B. W., I. C. Willis, M. J. Sharp, and N. S. Arnold (2000a), Modelling seasonal and spatial variations in the surface energy balance of Haut Glacier d'Arolla, Switzerland, *Ann. Glaciol.*, *31*, 53–62.

Brock, B. W., I. C. Willis, and M. J. Sharp (2000b), Measurement and parameterisation of albedo variations at Haut Glacier d'Arolla, Switzerland, *J. Glaciol.*, *46*(155), 675–688.

Brock, B. W., C. Mihalcea, M. P. Kirkbride, G. Diolaiuti, M. E. J. Cutler, and C. Smiraglia (2010), Meteorology and surface energy fluxes in the 2005–2007 ablation seasons at the Miage debris-covered glacier, Mont Blanc Massif, Italian Alps, *J. Geophys. Res.*, *115*, D09106, doi:10.1029/2009JD013224.

Carenzo M., F. Pellicciotti, and P. Burlando (2011), Mass balance modelling on Haut Glacier d'Arolla, Switzerland: How different levels of complexity of process representation affect predictions, Abstract C33B-0649 presented at 2011 Fall Meeting, AGU, San Francisco, Calif., 5–9 Dec. 2011.

Corripio, C. (2002), Modelling the energy balance of high altitude glacierised basins in the Central Andes, PhD thesis, Univ. of Edinburgh, Edinburgh, U. K.

Dadic, R., J. Corripio, and P. Burlando (2008), Mass-balance estimates for Haut Glacier d'Arolla, Switzerland, from 2000 to 2006 using DEMs and distributed mass-balance modeling, *Ann. Glaciol.*, *49*, 22–26.

Foster, L. A., B. W. Brock, M. E. J. Cutler, and F. Diotri (2012), A physically-based method for estimating supraglacial debris thickness from thermal band remote sensing data, *J. Glaciol.*, *58*(210), 677–691.

Fountain, A. G., M. Tranter, T. H. Nylen, K. J. Lewis, and D. R. Mueller (2004), Evolution of cryoconite holes and their contribution to meltwater runoff from glaciers in the McMurdo Dry Valleys, Antarctica, *J. Glaciol.*, *50*(168), 35–45.

Granger, R. J., J. W. Pomeroy, and J. Parviainen (2002), Boundary layer integration approach to advection of sensible heat to a patchy snow cover, paper presented at 59th Eastern Snow Conference, Stowe, Vermont.

Hubbard, A., H. Blatter, P. Nienow, D. Mair, and B. Hubbard (1998), Comparison of a three-dimensional model for glacier flow with field data from Haut Glacier db Arolla, Switzerland, *J. Glaciol.*, *44*(147), 368–378.

Intergovernmental Panel on Climate Change (2007), *Climate Change 2007: The Physical Science Basis. Contribution of Working Group I to the Fourth Assessment Report of the Intergovernmental Panel on Climate Change*, edited by S. Solomon et al.,Cambridge Univ. Press, Cambridge, U. K.

Kellerer-Pirklbauer, A. (2008), The supraglacial debris system at the Pasterze glacier, Austria: Spatial distribution, characteristics and transport of debris, *Z. Geomorphol. Suppl.*, *52*(1), 3–25.

Kirkbride, M. P. (1993), The temporal significance of transitions from melting to calving termini at glaciers in the central Southern Alps of New Zealand, *Holocene*, *3*(3), 232–240.

Klok, E. J., and J. Oerlemans (2002), Model study of the spatial distribution of the energy and mass balance of Morterartschgletscher, Switzerland, *J. Glaciol.*, *48*(163), 505–518.

Kossmann, M., A. P. Sturman, P. Zawar-Reza, H. A. McGowan, A. J. Oliphant, I. F. Owens, and R. A. Spronken-Smith (2002), Analysis of the wind field and heat budget in an alpine lake basin during summertime fair weather conditions, *Meteorol. Atmos. Phys.*, *81*, 27–52.

Lhomme, J. P., J. J. Vacher, and A. Rocheteau (2007), Estimating downward long-wave radiation on the Andean Altiplano, *Agric. For. Meteorol.*, *145*, 139–148.

MacDougall, F., and G. Flowers (2011), Spatial and temporal transferability of a distributed energy-balance glacier melt model, *J. Clim.*, *24*(202), 1480–1498.

Michlmayr, G., M. Lehning, G. Koboltschnig, H. Holzmann, M. Zappa, R. Mott, and W. Schoner (2008), Application of the Alpine 3D model for glacier mass balance and glacier runoff studies at Goldbergkees, Austria, *Hydrol. Processes*, *22*, 3941–3949.

Mihalcea, C., B. W. Brock, G. Diolaiuti, C. D'Agata, M. Citterio, M. P. Kirkbride, M. E. J. Cutler, and C. Smiraglia (2008), Using ASTER satellite and ground-based surface temperature measurements to derive supraglacial debris cover and thickness patterns on Miage Glacier (Mont Blanc Massif, Italy), *J. Cold Reg. Sci. Technol.*, *52*(3), 341–354.

Nakawo, M., and G. J. Young (1981), Field experiments to determine the effect of a debris layer on ablation of glacier ice, *Ann. Glaciol.*, *2*, 85–91.

Nicholson, L., and D. I. Benn (2006), Calculating ice melt beneath a debris layer using meteorological data, *J. Glaciol.*, *52*(178), 463–470.

Oerlemans, J., et al. (1998), Modelling the response of glaciers to climate warming, *Clim. Dyn.*, *14*, 267–274.

Østrem, G. (1959), Ice melting under a thin layer of moraine, and the existence of ice cores in moraine ridges, *Geogr. Ann.*, *41*(4), 228–230.

Pellicciotti, F., B. Brock, U. Strasser, P. Burlando, M. Funk, and J. Corripio (2005), An enhanced temperature-index glacier melt model including the shortwave radiation balance: Development and testing for Haut Glacier d'Arolla, Switzerland, *J. Glaciol.*, *51*(175), 573–587.

Pellicciotti, F., M. Carenzo, J. Helbing, S. Rimkus, and P. Burlando (2009), On the role of subsurface heat conduction in glacier energy-balance modelling, *Ann. Glaciol.*, *50*(50), 16–24.

Pellicciotti, F., T. Raschle, T. Huerlimann, M. Carenzo, and P. Burlando (2011), Transmission of solar radiation through clouds on melting glaciers: A comparison of parameterisations and their impact on melt modelling, *J. Glaciol.*, *57*(202), 367–381.

Petersen, L., and F. Pellicciotti (2011), Spatial and temporal variability of air temperature on a melting glacier: Atmospheric controls, extrapolation methods and their effect on melt modeling, Juncal Norte Glacier, Chile, *J. Geophys. Res.*, *116*, D23109, doi:10.1029/2011JD015842.

Popovnin, V. V., and A. V. Rozova (2002), Influence of sub-debris thawing on ablation and runoff of the Djankuat glacier in the Caucasus, *Nord. Hydrol.*, *33*(1), 75–94.

Reid, T., and B. Brock (2010), An energy-balance model for debris-covered glaciers including heat conduction through the debris layer, *J. Glaciol.*, *56*(199), 903–916.

Reijmer, C., and R. Hock (2008), Internal accumulation on Storglaciären, Sweden, in a multi-layer snow model coupled to a distributed energy- and mass-balance model, *J. Glaciol.*, *54*(184), 61–72.

Rye, C. J., N. S. Arnold, I. C. Willis, and J. Kohler (2010), Modeling the surface mass balance of a high Arctic glacier using the ERA-40 reanalysis, *J. Geophys. Res.*, *115*, F02014, doi:10.1029/2009JF001364.

Scherler, D., B. Bookhagen, and M. R. Strecker (2011), Spatially variable response of Himalayan glaciers to climate change affected by debris cover, *Nat. Geosci.*, *4*, 156–159.

Shea, J. M., and R. D. Moore (2010), Prediction of spatially distributed regional-scale fields of air temperature and vapor pressure over mountain glaciers, *J. Geophys. Res.*, *115*, D23107, doi:10.1029/2010JD014351.

Shukla, A., R. P. Gupta, and M. K. Arora (2009), Estimation of debris cover and its temporal variation using optical satellite sensor data: A case study in Chenab basin, Himalaya, *J. Glaciol.*, *55*(191), 444–452.

Stokes, C. R., V. Popovnin, A. Aleynikov, S. D. Gurney, and M. Shahgedanova (2007), Recent glacier retreat in the Caucasus Mountains, Russia, and associated increase in supraglacial debris cover and supra-/proglacial lake development, *Ann. Glaciol.*, *46*, 195–203.

Strasser, U., J. Corripio, F. Pellicciotti, P. Burlando, B. Brock, and M. Funk (2004), Spatial and temporal variability of meteorological variables at Haut Glacier d'Arolla (Switzerland) during the ablation season 2001: Measurements and simulations,*J. Geophys. Res.*, *109*, D03103, doi:10.1029/2003JD003973.

Swinbank, W. C. (1963), Longwave radiation from clear skies, *Q. J. R. Meteorol. Soc.*, *89*, 339–348.

Tenchov, B. G., and T. K. Yanev (1986), Weibull distribution of particle sizes obtained by uniform random fragmentation, *J. Colloid Interface Sci.*, *111*(1), 1–7.

Turnipseed, A., P. Blanken, D. Anderson, and R. Monson (2002), Energy budget above a high-elevation subalpine forest in complex topography, *Agric. For. Meteorol.*, *110*, 177–201.

Zemp, M., M. Hoelzle, and W. Haeberli (2009), Six decades of glacier mass-balance observations: a review of the worldwide monitoring network, *Ann. Glaciol.*, *50*, 101–111.